DOI: 10.1002/ejic.200901036

# Synthesis of Three-Quarter-Sphere-Like γ-AlOOH Superstructures with High Adsorptive Capacity

You Zhu,[a] Hongwei Hou,*[a] Gangling Tang,[a] and Qingyuan Hu*[a]

**Keywords:** γ-AlOOH / Hydrothermal synthesis / Layered compounds / Chromium / Nitrosamines

Three-quarter-sphere-like γ-AlOOH superstructures were successfully fabricated by a simple hydrothermal route exploiting the layered hydroxide structure. Several techniques such as X-ray diffraction (XRD), FTIR spectroscopy, field-emission scanning electron microscopy (FE-SEM), transmission electron microscopy (TEM), DSC thermal analysis, and nitrogen adsorption/desorption measurements were used to characterize the products. The possible formation mechanism of the three-quarter-sphere-like structure was proposed and discussed. The γ-AlOOH superstructures have high Brunauer–Emmett–Teller (BET) surface area and high adsorptive capacity. On the basis of these properties, they could be potentially used for removing chromium ions from highly toxic pollutant solutions and harmful tobacco-specific nitrosamines (TSNAs) from cigarette smoke.

## Introduction

Three-dimensional (3D) superstructures have found widespread applications in catalysis, adsorption, ceramics, photonics, electrochemistry, and biomedicine over the past decades due to their specific morphologies and functions.[1] Various methods have been developed for fabricating 3D architectures, such as template,[2] sacrificial-template,[3] template-free,[4] and Au-assisted electrolysis methods.[5]

In addition, the 3D hydroxide superarchitectures could be easily obtained from the layered structure of hydroxides through hydrogen bonding and dipolar forces under controllable conditions. Wu et al. synthesized VOOH hollow curved architectures called "dandelions" by organizing as-formed building blocks of flakes by a simple hydrothermal method.[6] Qiao et al. reported the synthesis of flowerlike hollow core–shell $Co(OH)_2$ structures made by aggregation of cobalt hydroxide building clusters.[7] The synthesis of novel γ-AlOOH nanotubes by sticking and scrolling the metastable lamellar precursor was reported in our earlier published work.[8] Subsequently, Zhang et al. progressively synthesized a sequence of flowerlike 3D boehmite γ-AlOOH nanostructures with an ethanol/water solution by using the effect of hydrogen bonding on the surface of nanorods or nanostrips.[9] From previous studies of hydroxyoxides, we can reach the conclusion that the aggregation of the layered structure of hydroxides has been exploited as a promising tool for the controllable formation of 3D hydroxide superstructures.

Aluminum oxide hydroxide of various morphologies has been recognized as a versatile and efficient adsorbent due to its relatively large surface and mesoporous properties.[10] AlOOH materials, which can avoid aggregation and maintain the high specific surface areas when in contact with pollutant water, like other materials,[11] have been proved to be useful and of common use due to their low cost and high effectiveness. $Cr^{VI}$ ions are considered as primary highly toxic pollutants in water, which diminish the amount of freshwater and threaten the survival of mankind.[12] Up to now, some studies have utilized γ-AlOOH for the removal of primary highly toxic pollutants (hexavalent chromium ions) in aqueous solution.[12b,13] To the best of our knowledge, there has been no report in the existing literature concerning the direct use of complicated morphologies of γ-AlOOH for the reduction of the amount of hexavalent chromium in aqueous solution. The removal of tobacco-specific nitrosamines [TSNAs, *N*-nitrosonornicotine (NNN), *N*-nitrosoanatabine (NAT), *N*-nitrosoanabasine (NAB), and 4-(methylnitrosamino)-1-(3-pyridyl)-1-butanone (NNK)] from cigarette smoke has attracted growing interest over the past years in tobacco chemistry, because these four TSNAs have been demonstrated to be potent carcinogens in animal studies.[14] The design and preparation of new materials are crucial for removing carcinogenic compounds from tobacco smoke. However, to the best of our knowledge, up to now, the use of γ-AlOOH for the reduction of the amount of TSNAs in tobacco smoke has not been reported.

[a] China National Tobacco Quality Supervision & Test Center, Zhengzhou Tobacco Research Institute of CNTC,
No. 2 Fengyang Street, Zhengzhou High & New Technology Industries Development Zone, Zhengzhou 450001, People's Republic of China
Fax: +86-371-67672625
E-mail: houhw@ztri.com.cn

In this work, a simple hydrothermal route was developed to synthesize three-quarter-sphere-like γ-AlOOH superstructures from the layered structure of hydroxides. XRD patterns, TEM images, FE-SEM images, FTIR spectra, DSC curves, and nitrogen adsorption/desorption measurements were used to characterize the products. In principle, the formation of inner-sphere surface complexes leads to disordering of the solid surface, the newly formed surfaces thereby becoming available for adsorption processes. These results demonstrated that the three-quarter-sphere-like γ-AlOOH architectures exhibited high Brunauer–Emmett–Teller (BET) surface area and excellent adsorptive capacity, implying that the prepared three-quarter-sphere-like γ-AlOOH superstructures could be potential adsorbents for chromium ions in contaminated water and harmful TSNAs in tobacco smoke.

## Results and Discussion

Figure 1(a) shows the typical XRD patterns of the as-obtained sample formed at 140 °C over 12 h. When compared to the standard pattern, all the diffraction peaks can be easily indexed to the orthorhombic AlOOH (JCPDS Card No. 21-1307), and no peaks from other phases can be observed. Further characteristics of three-quarter-sphere-like γ-AlOOH superstructures are also observed in the FTIR spectra shown in Figure 2. The shoulder at 3460 $cm^{-1}$ and the weak band at 1630 $cm^{-1}$ can be assigned to the stretching and bending modes of the adsorbed water, respectively.[15] The intense bands at 3310 and 3100 $cm^{-1}$ belong to the $\upsilon_{as}$(Al)O–H and $\upsilon_{s}$(Al)–H stretching vibrations, respectively.[10d] The 3310 and 3100 $cm^{-1}$ peaks of the as-prepared sample at 140 °C were concealed by the peak of adsorbed water. This phenomenon can be interpreted by comparing the curves of different samples obtained at different temperatures. The band at 1070 $cm^{-1}$ is assigned to the δsAl–O–H of γ-AlOOH.[10f] The torsional modes at 753, 641, and 478 $cm^{-1}$ of γ-AlOOH are also observed in the spectrum.[8] As the reaction temperature is raised, the intensities of all the bands that belong to γ-AlOOH increase, which indicates that the crystallinity is much better at a higher temperature. The band at 1380 $cm^{-1}$ is due to the characteristic stretching vibration of $NO_3^-$ resulting from the adsorbed $NH_4NO_3$ on the samples.[16]

The morphologies of the as-prepared γ-AlOOH were studied by field-emission scanning electron microscopy (FE-SEM) and transmission electron microscopy (TEM), and the images are shown in Figure 3. Figures 3(a) and (b) show the panoramic and magnified images of γ-AlOOH, respectively. The samples consist of uniform three-quarter-sphere-like structures almost to 100%. Further information in Figure 3(c) confirms that the three-quarter-sphere-like superstructures are made up of nanoplates with an average diameter of about 1 μm. The lateral TEM image [Figure 3(d)] distinctly shows the three-quarter-sphere-like structures. In the TEM images [Figure 3(e)], we also notice that there are parts missing in the sphere-like structures.

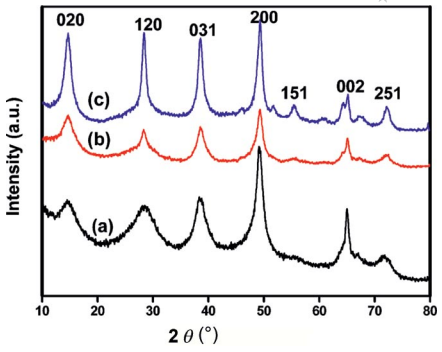


Figure 1. XRD patterns of the as-prepared samples formed at different temperatures over 12 h: (a) 140 °C, (b) 160 °C, (c) 180 °C.

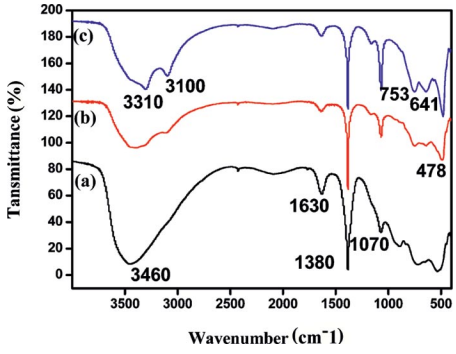


Figure 2. FTIR spectra of the products obtained over 12 h at different temperatures: (a) 140 °C, (b) 160 °C, (c) 180 °C.

The SAED pattern [inset of Figure 3(e)] taken randomly from the thin zone and the discontinuous rings illustrates the polycrystalline nature of the sample.[10d] The magnified HRTEM image [Figure 3(f)] shows the lattice spacing of about 0.314 nm, approximately corresponding to the (120) plane of the γ-AlOOH crystal.

With the intention of studying the effect of synthesis temperature on the morphologies, the temperatures were set at 160 and 180 °C. The corresponding XRD patterns are shown in Figures 1(b) and (c), respectively. Compared with the patterns of the sample at 140 °C, the crystallinity improved with an increase in the reaction temperature. From the FE-SEM and TEM images of samples prepared at 160 and 180 °C (Figure 4), we can clearly see that the morphologies are different from those of the sample synthesized at 140 °C. As the temperature was increased, the width of the sublevel structure nanoplates became smaller. The lengths of the long axes of the two superstructures obtained at 160 and 180 °C are all approximately 2 μm. It is clear that the temperature played a decisive part in the morphologies of three-quarter-sphere-like superstructures.

In order to investigate the growth process of the three-quarter-sphere-like superstructures, a series of comparative experiments at different reaction times were carried out. Only when reaction time reached 4 h, could we obtain a little product, whose FE-SEM image is shown in Fig-

  

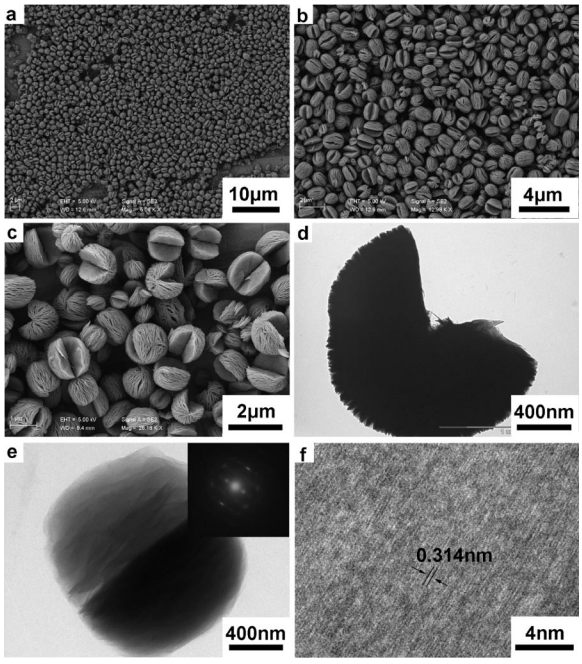


Figure 3. FE-SEM and TEM images of the three-quarter-sphere-like γ-AlOOH superstructures formed at 140 °C over 12 h: (a, b) panoramic FE-SEM images, (c) magnified FE-SEM images, (d) TEM image of selected three-quarter-sphere-like sample, (e) a panoramic TEM image with the corresponding SAED pattern, (f) a magnified HRTEM image.

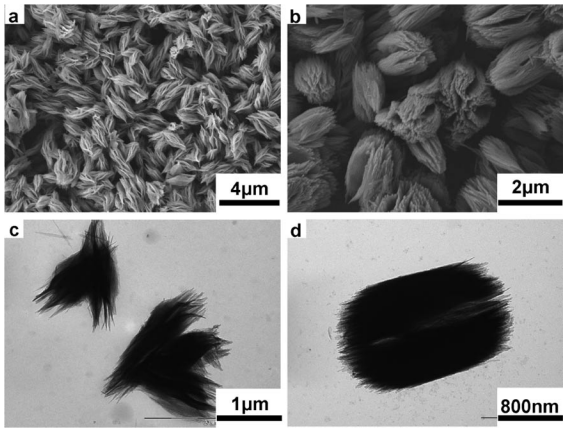


Figure 4. Structure and morphologies of γ-AlOOH structures formed over 12 h: FE-SEM images of samples prepared at 160 (a) and 180 °C (b); TEM images of samples prepared at 160 °C (c) and 180 °C (d).

ure 5(a). After 4 h, peanut-like structures with a length of 1 μm could be obtained. At 6 h, the widths of the peanut-like structures grew, and their subordinate structure changed as shown in Figure 5(b). Then at 7 h, the rudiments of the three-quarter-sphere-like AlOOH were visible [Figure 5(c)]. It was surprising that the missing parts of the spheres were less than a quarter. As the reaction time was increased to 8 h, as shown in Figure 5(d), the missing part gradually increased to one quarter. At a reaction time of 10 h, the morphology of the product was almost regularly three-quarter-sphere-like, as shown in Figure 5(f). At longer reaction times of up to 24 h, the morphologies did not change any more.

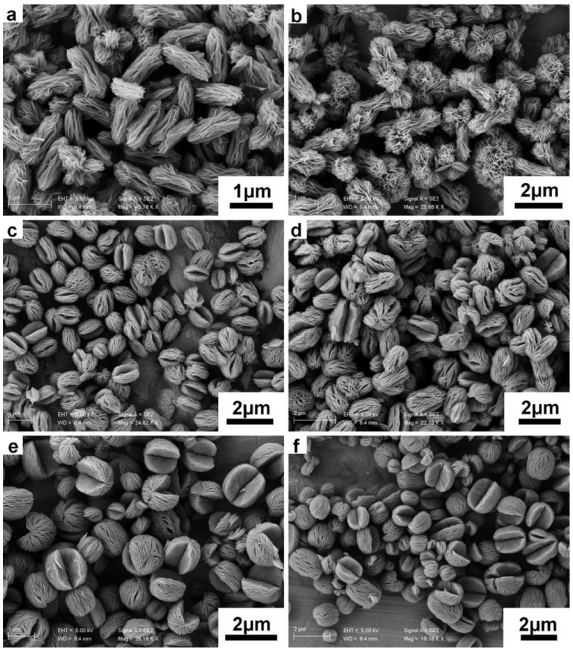


Figure 5. FE-SEM images of the γ-AlOOH structures formed at 140 °C over different reaction times: (a) 4 h, (b) 6 h, (c) 7 h, (d) 8 h, (e) 9 h, and (f) 10 h.

When the reaction reached the set time for the particular experiment, the system was cooled immediately with water, and the pH was measured. Through this method, we got the pH values of the reaction system at 2, 3, 4, 5, and 12 h, which were 3.7, 4.0, 4.2, 4.2, and 4.2, respectively. In acidic initial conditions of pH = 2.5, the decomposition of urea was fast and gradually slowed down when the pH was increased by the decomposed ammonia. Before 4 h, we obtained only a little product, which could mean that the decomposition of urea plays an important role in the growth process. After 4 h at 140 °C, all the urea decomposed completely, which adjusted the pH to 4.2. The main reactions of the three-quarter-sphere-like γ-AlOOH superstructures are shown in the following equations:

$$Al(NO_3)_3 + 3H_2O \rightarrow Al^{3+} + 3H^+ + 3OH^- + 3NO_3^- \text{ (pH = 2.5)} \quad (1)$$

$$CO(NH_2)_2 + H_2O \rightarrow 2\ NH_3 + CO_2\uparrow \quad (2)$$

$$NH_3 + H_2O \rightarrow NH_4^+ + OH^- \quad (3)$$

$$H^+ + OH^- \rightleftharpoons H_2O \quad (4)$$

$$Al^{3+} + 3OH^- \rightarrow Al(OH)_3 \quad (5)$$

$$Al(OH)_3 \rightarrow \gamma\text{-AlOOH} + H_2O \text{ (pH = 4.2)} \quad (6)$$

At first, aluminum nitrate was dissolved in water existing in the ions and this resulted in a pH value of 2.5. With the increase in temperature, urea started to decompose with the coexistence of water and decomposed to ammonia and $CO_2$ gas. Then, the ammonia reacted with water and produced

  

hydroxy groups. The hydroxy groups, in turn reacted with protons, so that the pH of the reactive system increased. On the other hand, amorphous aluminum hydroxide [$Al(OH)_3$] formed with the hydroxy group. When the pH reached a certain value (pH 4.2), $Al(OH)_3$ was dehydrated and eventually grew into the crystal (γ-AlOOH). The effect of pH on the growth of γ-AlOOH at different reaction times is shown in Figure 6.

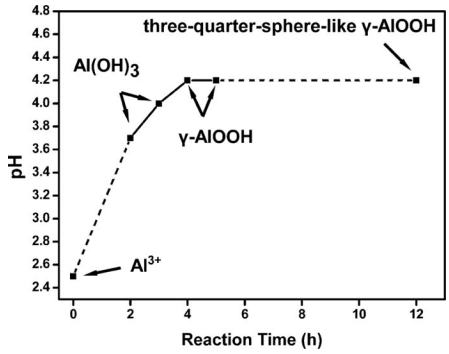


Figure 6. The effect of pH on the growth of γ-AlOOH at different reaction times.

The whole growth procedure was accomplished by the synergy of layered structures [as shown in Figure 7(a)], $NH_3$, $CO_2$, and asymmetric hydrogen bonding. The asymmetric hydrogen bonding caused the layered structure to assemble together. As the reaction proceeded, the decomposition of urea released $NH_3$ and $CO_2$, which adjusted the acidity and the pressure of the system, respectively, as well as controlling the morphologies. The formation of interstices in the layered structure was not only because of the hydrogen bonding but also owing to the effect of $CO_2$. With the increase in pH, the layered structure grew, as shown in Figure 7(b). Figure 7(c) shows the unstable structure which has over-three-quarter-sphere-like architecture. After the total decomposition of $CO(NH_2)_2$, the system was in thermodynamic and kinetic balance. In this airtight and balanced system, the layered structure ripened and formed the ultimate three-quarter-sphere-like morphologies, as shown in Figure 7(d). It is clear that $CO_2$ and the steady acidity (because there was no source of base) played important roles in the formation of the final structure.

Figure 8(a) shows the DSC thermal analysis of the as-prepared three-quarter-sphere-like γ-AlOOH superstructures. The sharp endothermic peaks at 120 °C may be attributed to the loss of $H_2O$ adsorbed by hydrogen bonding. At 325 °C, the γ-AlOOH tardily decomposed to γ-$Al_2O_3$. The broad peak around 380 °C may be caused by the adsorption of ammonium nitrate, whose existence was confirmed by IR spectroscopy. There were no other endothermic and exothermic peaks in the cooling curve of the first cycle, and the curve of the second cycle shows that the γ-AlOOH can quickly decompose to γ-$Al_2O_3$ at 500 °C. Accordingly, the sample calcined at 500 °C for 2 h can provide pure $Al_2O_3$, and the XRD patterns can be indexed to γ-$Al_2O_3$, as shown in Figure 8(b). The changes in the morphologies caused by calcination can be clearly seen in the SEM images shown in Figures 8(c) and (d). The morphologies change from three-quarter-like spheres to hemispheroid structures, but the layered configuration stays unchanged [Figure 7(e)]. Previous reports state that the outline of AlOOH nanorods[17] and nanotubes[15] stayed the same after calcination, whereas the structure of nanotubes became porous.

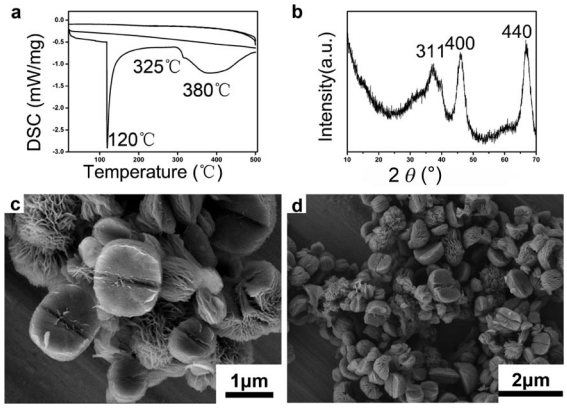


Figure 8. (a) DSC curves of the three-quarter-sphere-like γ-AlOOH superstructures formed at 140 °C over 12 h. (b) XRD patterns and (c,d) FE-SEM images of the sample decomposed from the three-quarter-sphere-like γ-AlOOH at 500 °C over 2 h.

$N_2$ adsorption/desorption measurements were conducted to examine the morphologies of the γ-AlOOH superstructure. These isotherms, together with the pore-volume distribution of the three-quarter-sphere-like products, are shown

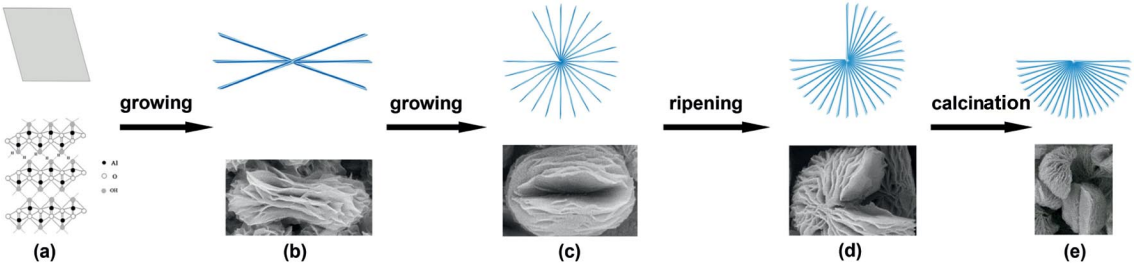


Figure 7. Suggested schematic diagram for the growth procedure of three-quarter-sphere-like γ-AlOOH superstructures: (a) an early metastable layered structure, (b) growing layered structures, (c) unstable structures growing further, (d) ultimate ripening of three-quarter-sphere-like morphologies, (e) changing into hemispheroids after calcination.

  

in Figure 9. The BET surface area of as-prepared sample was about 47.98 $m^2$/g, as calculated from the $N_2$ adsorption/desorption isotherms. Barrett–Joyner–Halenda (BJH) calculations for the pore-size distribution, derived from desorption data, revealed a narrow distribution centered at 10–11 nm for the three-quarter-sphere-like γ-AlOOH superstructures.

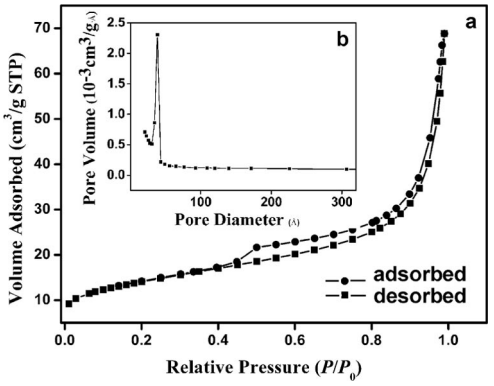


Figure 9. (a) Nitrogen adsorption/desorption isotherms and (b) pore-size distribution of the three-quarter-sphere-like γ-AlOOH superstructures.

The capacity of γ-AlOOH to adsorb $Cr^{VI}$ was investigated by mixing a certain amount of three-quarter-sphere-like γ-AlOOH superstructures with potassium dichromate solution of concentration varying from 4.86 μg/mL to 29.19 μg/mL. The percentage of chromium adsorbed by the γ-AlOOH superstructures was used to characterize the adsorption capacity of γ-AlOOH for $Cr^{VI}$, which is defined as:[13]

$$\%\,\text{adsorption} = \frac{c_0 - c_e}{c_0} \times 100 \quad (7)$$

where $c_0$ and $c_e$ denote the initial and final concentrations of $Cr^{VI}$ ions, respectively. When the concentration of $Cr^{VI}$ is lower than 14.60 μg/mL, 10 mg as-prepared three-quarter-sphere-like γ-AlOOH superstructures can efficiently adsorb more than 98% of the $Cr^{VI}$ ions present, which can be considered as nearly complete adsorption. When the concentration of $Cr^{VI}$ is higher than 14.60 μg/mL, the adsorption efficiency decreases with the increase in initial $Cr^{VI}$ concentration. It is clear that the as-prepared three-quarter-sphere-like γ-AlOOH superstructures reach saturation when the concentration of $Cr^{VI}$ is higher than 14.60 μg/mL. This maximum adsorption capacity of the three-quarter-sphere-like γ-AlOOH superstructures is about 25.9 μg/mg ($Cr^{VI}$/γ-AlOOH) at room temperature, which is an excellent capacity.

The adsorption capacity of three-quarter-sphere-like γ-AlOOH superstructures for $Cr^{VI}$ was calculated by using the Langmuir theory.[13]

$$\frac{c_e}{a_e} = \frac{1}{Ka_{max}} + \frac{c_e}{a_{max}} \quad (8)$$

In formula (8), $c_e$ is the equilibrium concentration of the $Cr^{VI}$ ions in solution (mol/L), $a_e$ represents the amount of chromium adsorbed at equilibrium (mol/g), $K$ and $a_{max}$ are Langmuir constants, the binding constant and the maximum adsorption capacity, respectively.[13] According to the formula, a linear plot was obtained that fits well with the Langmuir mode. The Langmuir constants $K$ ($1.835 \times 10^6$ $dm^3$/mol) and $a_{max}$ ($5 \times 10^{-5}$ mol/L) were obtained from the isotherm with a high correlation coefficient ($R^2$ = 0.9995). The result shows that the three-quarter-sphere-like γ-AlOOH superstructures have a higher maximum adsorption capacity than that reported by Granados-Correa et al. ($a_{max} = 5.432 \times 10^{-6}$ mol/L).[13]

Two experiments were carried out to investigate the adsorption capacity of the as-prepared three-quarter-sphere-like γ-AlOOH superstructures for tobacco-specific nitrosamines (TSNAs). The three-quarter-sphere-like γ-AlOOH superstructures were added into the cut tobacco and to the tips of cigarettes in order to study the removal of TSNAs from cigarette smoke. The amount of TSNAs in cigarette smoke was determined quantitatively by gas chromatography-thermal energy analysis (GC-TEA).

The decrease in the amounts of four TSNAs in cigarette smoke by adding three-quarter-sphere-like γ-AlOOH superstructures into cut tobacco is shown in Table 1. Compared with "blank" cigarettes (having no γ-AlOOH), the TSNA contents of cigarettes to which 10 mg/cigarette γ-AlOOH superstructures were added were selectively reduced without changing the tar content, which may influence the cigarette smoke quality. The adsorptive capacity of γ-AlOOH for NNN, NAT, NAB, and NNK is 61.5%, 50.2%, 26.5%, and 59.6%, respectively. Because the γ-AlOOH could block the N–NO group, which hampers the formation of TSNAs,[18] the three-quarter-sphere-like γ-AlOOH superstructures added into the cut tobacco not only influence cigarette combustion, but also work as adsorbents that reduce the amount of TSNAs. When AlOOH with complicated morphology was added into the wet tobacco, chemical transitions took place during the burning. At an added amount of 20 mg/cigarette, we found that the AlOOH had little effect on the amount of TSNAs. However, when the amount added was increased to 30 mg/cigarette, a big negative effect appeared. An appropriate amount of three-quarter-sphere-like γ-AlOOH added into the tobacco has a remarkable effect on the amount of TSNAs in cigarette smoke. When the added amount is much higher than the appropriate amount, the dehydration of AlOOH and the concomitant change in morphology may have an indefinite effect on the burning system.

The removal of four TSNAs from cigarette smoke by adding three-quarter-sphere-like γ-AlOOH superstructures to the tip of cigarettes is shown in Table 2. Compared with "blank" cigarettes, the amounts of the four TSNAs were obviously decreased by γ-AlOOH superstructures added to the tips of the cigarettes without changing the tar content. With increasing dosage of γ-AlOOH superstructures, the reduction of NNN basically remained the same. When the amount of γ-AlOOH superstructures added to the tips was 20 mg/cigarette, the adsorptive capacity of γ-AlOOH superstructures for NNK was 57.6%. The γ-AlOOH superstruc-

  

Table 1. The decrease in the amount of four TSNAs in cigarette smoke achieved by using three-quarter-sphere-like γ-AlOOH superstructures in cut tobacco.

| Amount of γ-AlOOH superstructures | NNN (ng/cigarette) | Reduction (%) | NAT (ng/cigarette) | Reduction (%) | NAB (ng/cigarette) | Reduction (%) | NNK (ng/cigarette) | Reduction (%) |
|---|---|---|---|---|---|---|---|---|
| Blank | 23.43 | – | 26.99 | – | 2.75 | – | 23.17 | – |
| 10 mg/cigarette | 9.01 | 61.5 | 13.43 | 50.2 | 2.02 | 26.5 | 9.37 | 59.6 |
| 20 mg/cigarette | 23.51 | –0.3 | 28.92 | –7.2 | 2.78 | –1.1 | 23.20 | –0.1 |
| 30 mg/cigarette | 22.11 | 5.6 | 36.42 | –34.9 | 3.73 | –35.6 | 23.91 | –3.2 |

Table 2. The decrease in the amount of four TSNAs in cigarette smoke achieved by using three-quarter-sphere-like γ-AlOOH superstructures in the tip of cigarettes.

| Amount of γ-AlOOH superstructures | NNN (ng/cigarette) | Reduction (%) | NAT (ng/cigarette) | Reduction (%) | NAB (ng/cigarette) | Reduction (%) | NNK (ng/cigarette) | Reduction (%) |
|---|---|---|---|---|---|---|---|---|
| Blank | 14.68 | – | 21.39 | – | 4.83 | – | 8.39 | – |
| 10 mg/cigarette | 13.00 | 11.4 | 15.94 | 25.5 | 3.61 | 25.3 | 5.09 | 39.3 |
| 20 mg/cigarette | 13.01 | 11.4 | 17.01 | 20.5 | 4.21 | 12.8 | 3.56 | 57.6 |
| 30 mg/cigarette | 13.04 | 11.2 | 19.05 | 10.9 | 4.10 | 15.1 | 5.43 | 35.3 |

tures in the tip of cigarettes were used as adsorbents for the H···N–NO hydrogen bonding due to their high BET surface area.

## Conclusion

A simple hydrothermal route was developed to synthesize three-quarter-sphere-like γ-AlOOH superstructures. The effects of reaction temperature and reaction time on the structures were systematically studied and tested by several techniques. This study revealed that the decomposition of urea along with the change in acidity played a crucial role on the formation of the architectures. Adsorption of $Cr^{VI}$ by these superstructures from toxic pollutant solutions was investigated and fits the Langmuir mode well. The reduction of the amount of TSNAs in tobacco smoke achieved by these materials shows that they have a potential application in the tobacco industry.

## Experimental Section

All chemical reagents were of analytical grade and were used as purchased from the Shanghai Chemical Reagent Company (P. R. China) without further purification. In a typical synthesis, $Al(NO_3)_3{\cdot}9H_2O$ (13 mmol) and $CO(NH_2)_2$ (16 mmol) were dissolved in deionized water (70 mL), and the resulting mixture was stirred for several minutes until it formed a clear solution. The solution was transferred into a Teflon-lined stainless-steel autoclave, then sealed and kept in the oven at 140 °C. After 12 h, the autoclave was slowly air-cooled to room temperature. The colloidal product was centrifuged and washed several times with deionized water followed by ethanol. Finally, the product was dried at 55 °C in vacuo for 12 h.

The phase identification of the samples was carried out on X-ray powder diffraction (XRD) patterns, by using a Philips X'pert X-ray diffractometer equipped with Cu-$K_a$ radiation ($\lambda$ = 1.54056 Å) employing a scanning rate of 10°min$^{-1}$. Fourier transform infrared (FTIR) spectra were obtained with a MAGNA IR-750 FT spectrometer. The morphologies of the samples were studied by field-emission scanning electron microscopy (FE-SEM, JEOL JSM-6700F), transmission electron microscopy (TEM, JEOL JEM-7650F), and high-resolution TEM (HRTEM, JEOL-2010). DSC thermal analysis was performed with NETZSCH DSC 200F3 at a heating rate of 10 °C/min from 20 °C to 500 °C and a cooling rate of 10 °C/min under a $N_2$ flow of 20 mL/min. The nitrogen adsorption and desorption isotherms at 77 K were measured with a Micrometrics ASAP 2020 analyzer. Before measurement, the samples were degassed in vacuo at 140 °C for at least 6 h.

The $Cr^{VI}$ adsorption experiments were carried out by mixing a certain amount of γ-AlOOH and potassium dichromate (20 mL) solution in airtight vials. After shaking for 1 h, the mixture was centrifuged for 3 min. The upper transparent solution was collected and analyzed by an inductively coupled plasma atomic emission spectrometer (ICP-AES, Thermo Ash Jarrell Corporation, Atomscan Advantage). All the experiments were carried out at room temperature.

The tobacco-specific nitrosamine (TSNA) contents of cigarettes were determined by combined gas chromatography and thermal energy analysis (GC-TEA 610). For the wet cut tobacco, a certain amount of three-quarter-sphere-like γ-AlOOH superstructures were dispersed in water to form an emulsion with a concentration of 50 g/L, and then the cut tobacco was sprayed with different volumes of emulsion to obtain proportions of 10, 20, and 30 mg/cigarette. The wet cut tobacco samples were dried at 40 °C until the moisture content was about 12%. The cut tobacco treated in this way was used to make cigarettes whose weight was 850 ± 30 mg by an automated process. For the dried material inserted into the tips of cigarettes, a certain amount of three-quarter-sphere-like γ-AlOOH superstructures were dispersed in the tips of cigarettes at proportions of 10, 20, and 30 mg/cigarette. Before smoking, the cigarettes were conditioned at 295 ± 1 K and 60 ± 2% relative humidity for 48 h and then smoked by a Cerulean SM 450 smoking machine under the standard ISO regime (ISO 4387).

## Acknowledgments

This work was supported by the National Nature Science Foundation of China (20701040).

[1] a) H. Han, R. B. Bai, *Ind. Eng. Chem. Res.* **2009**, *48*, 2891–2898; b) W. S. Wang, L. Zhen, C. Y. Xu, W. Z. Shao, *Cryst. Growth Des.* **2009**, *9*, 1558–1568.

  

[2] a) J. G. Yu, W. Liu, H. G. Yu, *Cryst. Growth Des.* **2008**, *8*, 930–934; b) T. R. Zhang, Q. Zhang, J. P. Ge, J. GoebI, M. W. Sun, Y. S. Yan, Y. S. Liu, C. L. Chang, J. H. Guo, Y. D. Yin, *J. Phys. Chem. C* **2009**, *113*, 3168–3175; c) C. L. Yan, D. F. Xue, *Funct. Mater. Lett.* **2008**, *1*, 37–42.
[3] a) J. J. Miao, L. P. Jiang, C. Liu, J. M. Zhu, J. J. Zhu, *Inorg. Chem.* **2007**, *46*, 5673–5677; b) Q. Gong, X. F. Qian, P. L. Zhou, X. B. Yu, W. M. Du, S. H. Xu, *J. Phys. Chem. C* **2007**, *111*, 1935–1940; c) Y. J. Gao, X. H. Hou, Q. F. Mo, C. Y. Wei, X. B. Qin, *J. Alloys Compd.* **2007**, *441*, 241–245.
[4] a) F. Liu, D. F. Xue, *Nanosci. Nanotechnol. Lett.* **2009**, *1*, 66–71; b) Y. F. Zhu, D. H. Fan, W. Z. Shen, *J. Phys. Chem. C* **2007**, *111*, 18629–18635; c) L. S. Zhong, J. S. Hu, A. M. Cao, Q. Liu, W. G. Song, L. J. Wan, *Chem. Mater.* **2007**, *19*, 1648–1655; d) L. P. Zhu, G. H. Liao, Y. Yang, H. M. Xiao, J. F. Wang, S. Y. Fu, *Nanoscale Res. Lett.* **2009**, *4*, 550–557; e) C. Yan, D. F. Xue, L. J. Zou, *Mater. Res. Bull.* **2006**, *41*, 2341–2348; f) J. S. Xu, D. F. Xue, Y. C. Zhu, *J. Phys. Chem. B* **2006**, *110*, 11232–11236.
[5] R. Bardhan, O. Neumann, N. Mirin, H. Wang, N. J. Halas, *Acs Nano* **2009**, *3*, 266–272.
[6] C. Z. Wu, Y. Xie, L. Y. Lei, S. Q. Hu, C. Z. OuYang, *Adv. Mater.* **2006**, *18*, 1727–1732.
[7] R. Qiao, X. L. Zhang, R. Qiu, J. C. Kim, Y. S. Kang, *Chem. Eur. J.* **2009**, *15*, 1886–1892.
[8] H. W. Hou, Y. Xie, Q. Yang, Q. X. Guo, C. R. Tan, *Nanotechnology* **2005**, *16*, 741–745.
[9] J. Zhang, S. J. Liu, J. Lin, H. S. Song, J. J. Luo, E. M. Elssfah, E. Ammar, Y. Huang, X. X. Ding, J. M. Gao, S. R. Qi, C. C. Tang, *J. Phys. Chem. B* **2006**, *110*, 14249–14252.
[10] a) P. Raybaud, M. Digne, R. Iftimie, W. Wellens, P. Euzen, H. Toulhoat, *J. Catal.* **2001**, *201*, 236–246; b) S. C. Shen, W. K. Ng, Q. Chen, X. T. Zeng, R. B. H. Tan, *Mater. Lett.* **2007**, *61*, 4280–4282; c) Y. Y. Li, J. P. Liu, Z. J. Ha, *Mater. Lett.* **2006**, *60*, 3586–3590; d) X. Y. Chen, H. S. Huh, S. W. Lee, *Nanotechnology* **2007**, *18*, 285608–285613; e) D. B. Kuang, Y. P. Fang, H. Q. Liu, C. Frommen, D. Fenske, *J. Mater. Chem.* **2003**, *13*, 660–662; f) Y. L. Feng, W. C. Lu, L. M. Zhang, X. H. Bao, B. H. Yue, Y. Iv, X. F. Shang, *Cryst. Growth Des.* **2008**, *8*, 1426–1429.
[11] a) C. Zamani, X. Illa, S. Abdollahzadeh-Ghom, J. Morante, A. Romano Rodríguez, *Nanoscale Res. Lett.* **2009**, *4*, 1303–1308; b) J. Hou, G. Zuo, G. Shen, H. Guo, H. Liu, P. Cheng, J. Zhang, S. Guo, *Nanoscale Res. Lett.* **2009**, *4*, 1241–1246; c) S. K. Kansal, N. Kaur, S. Singh, *Nanoscale Res. Lett.* **2009**, *4*, 709–716.
[12] a) M. Szekeres, E. Tombacz, K. Ferencz, I. Dekany, *7th Conference on Colloid Chemistry in Memoriam Aladar Buzagh* **1996**, Eger, Hungary, pp. 319–325; b) L. M. Zhang, W. C. Lu, L. M. Yan, Y. L. Feng, X. H. Bao, J. P. Ni, X. F. Shang, Y. Lv, *Microporous Mesoporous Mater.* **2009**, *119*, 208–216.
[13] F. Granados-Correa, J. Jimenez-Becerril, *J. Hazard. Mater.* **2009**, *162*, 1178–1184.
[14] a) K. A. Wagner, N. H. Finkel, J. E. Fossett, I. G. Gillman, *Anal. Chem.* **2005**, *77*, 1001–1006; b) J. Wu, P. Joza, M. Sharifi, W. S. Rickert, J. H. Lauterbach, *Anal. Chem.* **2008**, *80*, 1341–1345; c) Y. Cao, L. Y. Shi, C. F. Zhou, Z. Y. Yun, Y. Wang, J. H. Zhu, *Environ. Sci. Technol.* **2005**, *39*, 7254–7259.
[15] C. L. Lu, J. G. Lv, L. Xu, X. F. Guo, W. H. Hou, Y. Hu, H. Huang, *Nanotechnology* **2009**, *20*, 215604.
[16] a) X. L. Du, Y. Q. Wang, X. H. Su, J. G. Li, *Powder Technol.* **2009**, *192*, 40–46; b) S. M. Zhang, H. C. Zeng, *Chem. Mater.* **2009**, *21*, 871–883.
[17] S. Wei, J. Zhang, A. Elsanousi, J. Lin, F. Shi, S. Liu, X. Ding, J. Gao, S. Qi, C. Tang, *Nanotechnology* **2007**, *18*, 255605.
[18] Y. Cao, Z. Yun, J. Yang, X. Dong, C. Zhou, T. Zhuang, Q. Yu, H. Liu, J. Zhu, *Microporous Mesoporous Mater.* **2007**, *103*, 352–362.

Received: October 26, 2009
Published Online: January 12, 2010

  